



HAL
open science

Sound velocities and density measurements of solid hcp-Fe and hcp-Fe-Si(9wt.%) alloy at high pressure: Constraints on the Si abundance in the Earth's inner core

Daniele Antonangeli, Guillaume Morard, Luigi Paolasini, Gaston Garbarino, Caitlin Murphy, Eric Edmund, Frédéric Decremps, Guillaume Fiquet, Alexei Bosak, Mohamed Mezouard, et al.

► To cite this version:

Daniele Antonangeli, Guillaume Morard, Luigi Paolasini, Gaston Garbarino, Caitlin Murphy, et al.. Sound velocities and density measurements of solid hcp-Fe and hcp-Fe-Si(9wt.%) alloy at high pressure: Constraints on the Si abundance in the Earth's inner core. *Earth and Planetary Science Letters*, 2018. hal-01921038

HAL Id: hal-01921038

<https://hal.sorbonne-universite.fr/hal-01921038>

Submitted on 13 Nov 2018

HAL is a multi-disciplinary open access archive for the deposit and dissemination of scientific research documents, whether they are published or not. The documents may come from teaching and research institutions in France or abroad, or from public or private research centers.

L'archive ouverte pluridisciplinaire **HAL**, est destinée au dépôt et à la diffusion de documents scientifiques de niveau recherche, publiés ou non, émanant des établissements d'enseignement et de recherche français ou étrangers, des laboratoires publics ou privés.

1 **Sound velocities and density measurements of solid hcp-Fe and hcp-Fe-Si(9wt.%) alloy**
2 **at high pressure: Constraints on the Si abundance in the Earth's inner core**

3

4 Daniele Antonangeli^{1,*}, Guillaume Morard¹, Luigi Paolasini², Gaston Garbarino², Caitlin A.
5 Murphy³, Eric Edmund¹, Frederic Decremps¹, Guillaume Fiquet¹, Alexei Bosak², Mohamed
6 Mezouar², Yingwei Fei³

7

8 ¹ Institut de Minéralogie, de Physique des Matériaux, et de Cosmochimie (IMPMC), UMR
9 CNRS 7590, Sorbonne Universités – UPMC, Muséum National d'Histoire Naturelle, IRD
10 unité 206, 75252 Paris, France.

11 ² European Synchrotron Radiation Facility, BP 220, 38043 Grenoble Cedex, France.

12 ³ Geophysical Laboratory, Carnegie Institution of Washington, Washington DC 20015, USA

13 * e-mail: daniele.antonangeli@impmc.upmc.fr

14

15

16 **Abstract**

17 We carried out sound velocity and density measurements on solid hcp-Fe and an hcp-
18 Fe-Si alloy with 9 wt.% Si at 300 K up to ~170 and ~ 140 GPa, respectively. The results
19 allow a precise determination of the dependence on density (ρ) of the compressional sound
20 velocity (V_P) and of the shear sound velocity (V_S) for pure Fe and the Fe-Si alloy. The
21 established V_P - ρ and V_S - ρ relations are used to address the effect of Si on the velocities in the
22 Fe-FeSi system in the range of Si concentrations 0 to 9wt.% applicable to the Earth's core.
23 Assuming an ideal linear mixing model, velocities vary with respect to those of pure Fe by ~
24 +80 m/s for V_P and ~ -80 m/s for V_S for each wt.% of Si at the inner core density of 13000
25 kg/m³. The possible presence of Si in the inner core and the quantification of its amount
26 strongly depend on anharmonic effects at high temperature and on actual core temperature.

27

28 **Keywords:** seismic wave velocities; iron; iron-silicon alloys; high pressure; high temperature;
29 Earth's inner core

30

31 **1. Introduction**

32 The physical properties of iron and iron alloys at high pressure are crucial to refine the
33 chemical composition and dynamics of the Earth's core. To this respect, density (ρ),
34 compressional-wave (V_P) and shear-wave (V_S) sound velocities are of particular importance,
35 as those parameters can be directly compared to the seismological observations.

36 Over the last twenty years, a great effort has been devoted to the development of
37 experiments capable of probing sound velocity of metallic samples at high pressure, with a
38 specific focus on iron (see *Antonangeli and Ohtani [2015]* for a recent review). Ab initio
39 calculations have been extensively applied as well to assess material's properties at core
40 pressures and temperatures [e.g. *Vočadlo et al., 2009; Sha and Cohen, 2010; Martorell et al.,*
41 *2013*]. Yet, a consensus has not been reached, not only concerning the absolute values of
42 velocities of solid iron at inner core conditions, but also the dependence of velocities upon
43 pressure and temperature.

44 Since the seminal work of *Birch [1952]* it has been well established that light elements
45 are alloyed to iron in the Earth's core to account for the density difference between pure Fe
46 and seismological observations (e.g. model PREM by *Dziewonski and Anderson [1981]*). For
47 the solid inner core, many recent experimental studies suggest silicon as one of the major
48 candidates, based on its physical properties (density and sound velocity) and/or affinity for the
49 metallic phase during Earth's differentiation [e.g. *Lin et al., 2003; Badro et al., 2007;*
50 *Antonangeli et al., 2010; Mao et al. 2012; Siebert et al., 2013; Fischer et al., 2015; Tateno et*
51 *al., 2015*]. However, different works propose different amount of Si alloyed to Fe in the inner
52 core, ranging from ~2wt.% [*Badro et al., 2007; Antonangeli et al., 2010*] up to ~8% [*Mao et*
53 *al. 2012; Fischer et al., 2015*]. One of the causes for such a discrepancy is the large pressure
54 and temperature extrapolation necessary to compare experimental results with inner core
55 seismological models. For instance, results based on linear extrapolations of V_P - ρ relation

56 argued for about 2 wt% Si alloyed to Fe in the inner core [Badro *et al.*, 2007; Antonangeli *et*
57 *al.*, 2010], while a model using a power law for the V_P - ρ extrapolation proposed 8 wt% Si
58 [Mao *et al.* 2012]. In contrast with the bulk of the experimental results, a very recent
59 computational work on silicon alloys at inner core conditions [Martorell *et al.*, 2016]
60 suggested that both the P-wave and the S-wave velocities of any hcp-Fe-Si alloy would be too
61 high to match the seismically observed values at inner-core density.

62 To shed light on this ongoing debate, we carried out sound velocity and density
63 measurements on pure Fe and a Fe-Si alloy with 9 wt.% Si in the hexagonal close-packed
64 structure (hcp) from ~40 GPa up to ~170 GPa, using inelastic x-ray scattering (IXS) and x-ray
65 diffraction (XRD). IXS allows a clear identification of longitudinal aggregate excitations in
66 polycrystalline samples [Fiquet *et al.*, 2001, 2009; Antonangeli *et al.*, 2004, 2010, 2012,
67 2015; Badro *et al.*, 2007; Mao *et al.*, 2012; Ohtani *et al.*, 2013] and the derivation of V_P from
68 a sine fit of the phonon dispersion. Combining the measured V_P with the bulk modulus
69 derived from the equation of state, V_S can be determined as well, while the density is directly
70 obtained from the collected diffraction patterns. In this study, we aim to establish precise
71 relations between velocities (both V_P and V_S) and density for Fe and a representative Fe-Si
72 alloy with 9 wt.% Si over a wide pressure range at room temperature. The results will provide
73 a reference benchmark for calculations and will serve as basis for further studies of increased
74 compositional complexity and evaluating the temperature effects on the velocities.

75

76 **2. Materials and Methods**

77 Starting materials consisted in commercially available polycrystalline samples of Fe
78 (99.998%, Alpha Aesar) and a Fe-Si alloy with 9 wt.% Si (Goodfellow, hereafter Fe-Si9).
79 Nominal composition and chemical homogeneity at micrometric scale of the Fe-Si alloy has
80 been verified by electron microprobe analysis.

81 IXS and XRD measurements have been carried out at the European Synchrotron
82 Radiation facility (ESRF) at ID28 and ID27 beamlines, respectively. IXS measurements have
83 been performed on polycrystalline specimens compressed in a diamond anvil cell (DAC)
84 using the Si(9,9,9) instrument configuration, which yields an overall energy resolution of 3
85 meV full width half maximum (FWHM). Absolute energies have been calibrated prior to the
86 experiment comparing IXS diamond phonon dispersion with that obtained by inelastic
87 neutron and Raman scattering. Specific to this experiment, we double-checked the energy
88 calibration by comparing the sound velocity measured by IXS on iron powders at ambient
89 conditions with the Voigt–Reuss–Hill average of ultrasonic determination on single crystal
90 [Guinan and Beshers, 1968]. We also calibrated the scattering angle at the small working
91 values of our IXS measurements by collection of diffraction from a silver behenate standard.
92 Optics in Kirkpatrick-Baez configuration allowed focusing the x-ray beam at sample position
93 at $30 \times 70 \mu\text{m}^2$ (horizontal x vertical, FWHM) or down to $12 \times 7 \mu\text{m}^2$ (horizontal x vertical,
94 FWHM) depending upon DAC configuration. Momentum resolution was set by slits in front
95 of the analyzers to 0.28 nm^{-1} and to 0.84 nm^{-1} , in the scattering plane and perpendicular to it.
96 A vacuum chamber was used to minimize the quasi-elastic scattering contribution from air.
97 Good-statistic data have been obtained with typical integration time of ~ 300 s per point for
98 Fe, and ~ 500 - 600 s per point for Fe-Si9.

99 Pressures were generated by symmetric type, MAO DAC, using composite Re/c-BN
100 gaskets, with either $150/300 \mu\text{m}$ beveled anvils, or $40/100/300 \mu\text{m}$ beveled anvils prepared by
101 focus ion beam (FIB) technique [Fei et al., 2016]. Diamonds were pre-aligned and oriented to
102 select the fastest transverse acoustic phonon of the diamond in the scattering plane and to
103 minimize its intensity. The focused beam of $12 \times 7 \mu\text{m}^2$ FWHM at sample position granted
104 collection of clean spectra on specimens down to $\sim 35 \mu\text{m}$ in diameter. Such a small beam also
105 permitted to probe phonons across moderate pressure gradients (as determined from the fine

106 diffraction mesh, see below), while the composite gasket ensured relatively thick samples (8
107 to 12 μm at the highest pressure), and hence proper IXS signal, averaged over a reasonably
108 large number of grains. Pressure was increased off line by monitoring the Raman spectra at
109 the tip of the diamonds, and more precisely measured by the x-ray diffraction according to
110 known samples equation of state. Specifically we used a third-order Birch-Murnaghan
111 formalism, with $V_0 = 22.47 \text{ \AA}^3/\text{unit cell}$ [Dewaele *et al.* 2006], $K_0 = 155 \text{ GPa}$ and $K' = 5.37$
112 [Sakai *et al.*, 2014] for hcp-Fe and $V_0 = 23.50 \text{ \AA}^3/\text{unit cell}$, $K_0 = 129 \text{ GPa}$ and $K' = 5.24$ for
113 hcp-Fe-Si9 [Fei, 2017].

114 At each investigated pressure point, we mapped the aggregate longitudinal acoustic
115 phonon dispersion throughout the entire first Brillouin zone collecting 6 to 9 spectra in the 3-
116 12.5 nm^{-1} range. The energy positions of the phonons were extracted by fitting a set of
117 Lorentzian functions convolved with the experimental resolution function to the IXS spectra.
118 Figure 1 shows an example of the collected IXS spectra and the fitted result. We derived V_P
119 from a sine fit to the phonon dispersion [Antonangeli *et al.*, 2004] (Figure 1), with error bars
120 between ± 1 and $\pm 3\%$ for Fe and between ± 2 and $\pm 4\%$ for Fe-Si9. The errors account for
121 statistical errors, finite energy and momentum resolution, as well as deviation from ideal
122 random orientation of the polycrystalline samples. Combining the measured V_P with bulk
123 modulus from the equation of state (the difference between isothermal and adiabatic bulk
124 modulus at 300 K is negligible), we also derived V_S [Antonangeli *et al.*, 2004], with
125 uncertainties, obtained by propagating uncertainties on V_P and on K (the contribution from
126 uncertainties on density was observed to be negligible), between ± 5 and $\pm 6\%$ for pure-Fe, and
127 between ± 8 and $\pm 10\%$ for Fe-Si9 (assuming different equation of state leads to effects on V_S
128 within reported error bars).

129 For both samples, we collected angle dispersive 2D diffraction patterns at each
130 investigated pressure point, with a monochromatic wavelength of 0.3738 \AA (iodine K edge).

131 This allowed for clear structure determination and direct measurements of samples' density.
132 Taking advantage of the $3 \times 3 \mu\text{m}^2$ beam, we mapped the entire sample area, monitoring
133 pressure gradients across the sample chamber. Diffraction data are also used to detect any
134 developed texture. An example of the collected diffraction patterns are shown in Figure 2 and
135 Figure 3. The diffraction patterns of the compressed hcp-Fe (Figure 2) show rather smooth
136 rings, indicating the small sizes of the diffracting crystallites (average size ~ 25 nm at 167
137 GPa) and the good orientation averaging (only 100 reflection shows some variation in
138 intensity with the azimuthal angle). Two-dimensional detector images caked into rectilinear
139 projection show negligible dependence of the d spacing on the azimuthal angle around $2\theta=0$
140 direction (Figure 2), and hence a negligible deviatoric stress [Wenk *et al.*, 2006]. Furthermore,
141 the (002) reflection, although weak, is still visible up to the highest attained pressure, further
142 highlighting the overall marginal preferential orientation. Such observations support the
143 overall validity of the random orientation approximation, critical to the analysis and
144 interpretation of the IXS results [Antonangeli *et al.*, 2004; Bosak *et al.*, 2007;2016]. The
145 diffraction patterns collected for the Fe-Si9 alloy (Figure 3) are somewhat less favorable than
146 those on pure Fe, in particular in term of sizes of crystallites (average size ~ 40 nm at 117
147 GPa) and randomness of the distribution (intensity variation are quite visible for both 100 and
148 101 reflections), but they are still acceptable. The (002) reflection, still visible at all probed
149 pressure, is very weak, as a direct consequence of a small preferential orientation fully
150 developed already at 59 GPa and not significantly evolving with pressure, with the c-axis
151 preferentially aligned along the main compression axis of the cell. Similar texture has been
152 already reported in previous experiments on iron [Wenk *et al.*, 2000] and other metals with
153 hcp structure [Merkel *et al.*, 2006]. Such a moderately increased deviation from the ideal
154 random distribution is reflected into the fairly increased error bars on the velocities derived
155 from the IXS data (deviation from ideal average up to 2%).

156 At the highest compression the maximum observed difference in pressure across the
157 sample chamber ($\sim 35 \mu\text{m}$) is $<7 \text{ GPa}$ for Fe and $<10 \text{ GPa}$ for Fe-Si9. Over the volume seen by
158 IXS we obtain an average pressure of 167 GPa (Fe), with a standard deviation of 2 GPa and a
159 standard error of 1 GPa , and an average pressure of 144 GPa (Fe-Si9), with a standard
160 deviation of 2 GPa and a standard error of 1 GPa .

161

162 **3. Results**

163 The experimentally determined densities and velocities for hcp-Fe and hcp-Fe-Si9 are
164 summarized in Table 1. The details are presented in the following subsections.

165 **3.1. Hcp-Fe**

166 The measured compressional and shear sound velocities as a function of density are
167 plotted in Figure 4. These new measurements of V_P are in very good agreement with the V_P - ρ
168 linear relationship recently proposed by fitting a combined datasets derived from multiple
169 techniques [Antonangeli and Ohtani, 2015], extending the data coverage at extreme pressures.
170 We notice that the extrapolation of the established trend to higher density is in remarkable
171 agreement with ab initio calculations at 0 K [Vočadlo et al., 2009; Sha and Cohen, 2010],
172 clearly supporting a linear dependence of V_P on density. The derived V_S - ρ linear relationship
173 is also in general agreement with results of ab initio calculations at 0 K . We also noticed the
174 good agreement between the slope of our V_S - ρ trend with that obtained by the most recent
175 nuclear resonant inelastic x-ray scattering (NRIXS) experiments [Murphy et al., 2013;
176 Gleason et al., 2013; Liu et al., 2016], even if actual V_S values derived by NRIXS are
177 somewhat lower, between 3 to 8% depending upon datasets. Such a difference is at least
178 partially due to the enrichment in heavier Fe isotopes of samples used for NRIXS studies with
179 respect to sample of natural isotopic abundance used here.

180 **3.2 Hcp-Fe-Si9**

181 The measured compressional and shear sound velocities as a function of density are
182 shown in Figure 5. Our V_P measurements on samples with 9 wt.% Si are very close to
183 previous IXS measurements on samples with 8 wt.% Si [Mao *et al.*, 2012], but they are
184 systematically higher than early determination by NRIXS on samples with 8 wt.% Si [Lin *et*
185 *al.*, 2003]. Similar to the case of pure Fe, our measurements support a linear dependence of
186 V_P on ρ for Fe-Si9. The derived V_S - ρ relationship can be well described by a second order
187 polynomial (Figure 5).

188 Comparison of results obtained for Fe and Fe-Si9 (Figure 6) show that Si alloying
189 systematically increases V_P at constant density over the investigated pressure range. Linear
190 fits indicate that, even if V_P of the Fe-Si9 alloy increases with density slower than pure Fe,
191 Fe-Si9 is still expected to have significantly higher V_P than Fe at inner core density (~ 12390
192 m/s vs. ~ 11680 m/s at 13000 kg/m^3). On the other hand, the derived density evolution for V_S
193 of Fe-Si9 is such that the Si-bearing alloys is expected to have higher V_S than pure Fe only up
194 to $\rho \approx 11200 \text{ kg/m}^3$, with V_S of Fe larger than V_S of Fe-Si9 at inner core density (~ 5130 m/s vs.
195 ~ 5890 m/s at 13000 kg/m^3). This trend (i.e V_P increasing with Si content and V_S decreasing)
196 has been reported as well by recent ab initio calculations of Fe-Si alloys at core pressures
197 [Martorell *et al.*, 2016]. On the contrary to the case of pure Fe, the extrapolation of our
198 experimental results for Fe-Si9 does not agree with the calculations.

199

200 **4. Discussion**

201 Concerning hcp-Fe, we note a remarkable agreement between our new measurements,
202 previous measurements by various techniques and ab initio calculations for V_P , and an overall
203 agreement for V_S . The established consensus provides very strong constraints on the linear

204 dependence of velocities on density and on actual values of velocities of hcp-Fe at inner core
205 densities and 300 K (Figure 4), which can by now be considered known within few percent
206 (with V_P better constrained than V_S).

207 Somewhat less evident is the case for Si bearing hcp Fe-alloys. Literature data obtained
208 in the ~40 to ~100 GPa range on samples of the same nominal composition [*Lin et al., 2003*;
209 *Mao et al., 2012*] are in evident disagreement (Figure 5). Reasons for the discrepancy
210 between NRIXS [*Lin et al., 2003*] and IXS [*Mao et al., 2012*] data possibly include
211 systematic differences due to the techniques, or due to the sample's texture. The V_P measured
212 in this study is in a good agreement with previous IXS determination at lower pressures [*Mao*
213 *et al., 2012*] and significantly extend the probed pressure range. In view of our new data, the
214 sub linear evolution of V_P with density according to the empirical power-law function
215 proposed by *Mao et al., [2012]* on the basis of V_P - ρ data over a more restricted pressure range,
216 seems not justified. Linear extrapolation of experimental results to inner core density and
217 comparison with calculations [*Tsuchiya and Fujibuki, 2009*; *Martorell et al., 2016*] show
218 however a disagreement, more important for V_P than for V_S . The difference would be even
219 more striking when considering a power-law extrapolation. In particular, the calculations
220 seem to overestimate the effect of Si on V_P of the Fe-Si alloys. We noticed that ab initio
221 calculations on Fe-Si alloys, even when performed at 0 K, give quite conflicting results
222 [*Tsuchiya and Fujibuki, 2009*; *Martorell et al., 2016*], highlighting the difficulty in
223 performing calculations taking into account the configurational order/disorder inherent to
224 alloys. Further investigation by both experiments and theoretical calculations is necessary to
225 resolve the discrepancy.

226 The direct comparison between results obtained on Fe and on Fe-Si9 allows us to
227 address the effect of Si content on the velocities of a hcp $Fe_{1-x}Si_x$ alloy in the limit of low to
228 moderate Si concentration (0 to 9wt.%). The simplest approach is to use an ideal linear

229 mixing model [e.g. *Badro et al., 2007; Antonangeli et al., 2010*]. Using the reference relations
230 established here for pure Fe and the extrapolation of our measurements on Fe-Si9, at the inner
231 core density of 13000 kg/m^3 we get a variation $\sim +80 \text{ m/s}$ on V_P and $\sim -80 \text{ m/s}$ on V_S for each
232 wt.% of Si (Figure 6). Measurements of V_P on an Fe-Ni-Si alloy with 4.3wt.% Ni and
233 3.7wt.% Si [*Antonangeli et al., 2010*] extrapolated to 13000 kg/m^3 yield $V_P \sim 12100 \text{ m/s}$, in
234 good agreement with our estimate of $V_P \sim 11980 \text{ m/s}$ for a Fe-Si alloy with 3.7wt.% Si
235 (difference $\sim -1\%$). This agreement on one side argues in favor of the suitability of the here-
236 proposed estimate, and on the other suggests that the effect on the compressional sound
237 velocity due to Ni inclusion at level of 4 to 5 wt.% is minor. Further independent support
238 comes from the good agreement also observed between our predicted value of $V_P \sim 12160 \text{ m/s}$
239 and the extrapolation of very new measurements on a Fe-Si alloy with 6wt.% Si [*Sakairi et al.,*
240 *Am. Min. in press.*] yielding $V_P \sim 11940 \text{ m/s}$ (difference $\sim +1.8\%$).

241 In order to be able to use our data to discuss the Si abundance in the inner core by
242 comparison with seismological models, the effects of high temperature have to be accounted
243 for. A velocity vs. density representation, as the one proposed here, implicitly accounts for
244 quasi-harmonic effects. Anharmonic effects might be important as well, in particular on V_S
245 and for temperatures approaching melting. Sound velocity measurements at simultaneous
246 high pressure and high temperature conditions are at the cutting edge of current technical
247 capabilities and only few datasets are available, mostly for pure Fe [e.g. *Antonangeli et al.,*
248 *2012; Mao et al., 2012; Ohtani et al., 2013; Sakamaki et al., 2015*]. If we model high-
249 temperature effects for Fe following *Sakamaki et al. [2015]*, V_P is expected to lower by $\sim -$
250 0.09 m/s K^{-1} at the constant density of 13000 kg/m^3 . The orange arrow in Figure 4 highlights
251 the magnitude of the expected reduction of V_P for T up to $\sim 7000 \text{ K}$. Alternatively we can
252 model temperature-induced softening (in this case for both V_P and V_S) following calculations
253 by *Martorell et al., [2013]*. As these calculations have been performed at constant pressure,

254 while here we are interested in the effects at constant density, we corrected the computed
255 values according to the measured density dependence of sound velocities to compensate for
256 the effects due to density variation with increasing temperature. Once limiting to T up to 7000
257 K, the estimated lowering of V_P and V_S are, respectively, ~ -0.12 m/s K^{-1} and ~ -0.32 m/s K^{-1}
258 at the constant density of 13000 kg/m³. The violet arrows in Figure 4 highlights the magnitude
259 of the expected reduction of V_P and V_S for T up to ~ 7000 K. In qualitative agreement with
260 recent calculations, for Fe, temperature effects alone seem enough to explain inner core
261 velocities (but not densities, too high for pressures in the 330 to 360 GPa range). In the case
262 of Fe-Si alloys we can only rely on calculations [Martorell *et al.*, 2016], which, once
263 corrected as in the case of Fe, yield for a sample with 3.2 wt% Si a reduction of V_P and V_S of,
264 respectively, ~ -0.12 m/s K^{-1} and ~ -0.34 m/s K^{-1} , and for a sample with 6.7 wt% Si a
265 reduction of ~ -0.20 m/s K^{-1} and ~ -0.23 m/s K^{-1} , at the constant density of 13000 kg/m³. We
266 note that theoretical estimates for pure Fe and a Fe-Si alloy with 3.2wt.% Si are very close,
267 while those for a Fe-Si with 6.7wt.% Si differ, with an effect on V_P almost double and an
268 effect on V_S about 30% smaller. The arrows in Figure 5 highlights the magnitude of the
269 expected reduction of V_P and V_S for T up to ~ 7000 K if we apply to the extrapolation to our
270 measurements on Fe-Si9 the correction estimated for samples with 3.2wt.% Si or that for
271 samples with 6.7 wt.% Si (the dark blue arrows in the first case, and green arrows in the
272 second case). Similarly to the case of Fe, if temperature effects are as large as expected
273 according to calculations, temperature alone might be enough to explain inner core velocities
274 (but again, not the densities, too low for pressures in the 330 to 360 GPa range for samples
275 with 9 wt.% Si [Tateno *et al.*, 2015]).

276 If we assume temperature effects at the constant density of 13000 kg/m³ of ~ -0.20 m/s
277 K^{-1} for V_P and ~ -0.23 m/s K^{-1} for V_S (as from estimates from calculations on a sample with
278 6.7 wt% Si) we match PREM values of V_P and V_S for a Si concentration of 10 ± 1 wt.% and T

279 between 6500 and 6700 K. This solution however is not acceptable, as such Fe-Si alloy is
280 expected to have the right density only for pressures well above 360 GPa [Tateno *et al.*, 2015].
281 If we assume temperature effects at the constant density of 13000 kg/m^3 of $\sim -0.12 \text{ m/s K}^{-1}$ for
282 V_P and $\sim -0.33 \text{ m/s K}^{-1}$ for V_S (as from estimates from calculations on pure Fe and on a
283 sample with 3.2 wt% Si) we obtain PREM values of V_P and V_S for a Si concentration of 3 ± 1
284 wt.% and T between 6200 and 6500 K. P-V-T relation for a Fe-Si alloy with ~ 3 wt.% Si has
285 not been experimentally determined yet, but calculations suggest such an alloy to have a
286 density of $\sim 13160 \text{ kg/m}^3$ at 360 GPa and 6400 K [Martorell *et al.*, 2016], thus making this
287 solution acceptable. Furthermore, an inner core temperature of 6200-6500 K is well
288 compatible with estimates based on measurements of the Fe and Fe-Si alloys melting curve
289 [Anzellini *et al.*, 2013; Morard *et al.*, 2011]. However, as already mentioned, the most recent
290 experimental determination of temperature dependence of V_P for Fe by Sakamaki *et al.*
291 [2016] argues for a less important temperature-induced lowering with respect to that proposed
292 by calculations. If we assume temperature effects at the constant density of 13000 kg/m^3 of \sim
293 -0.09 m/s K^{-1} for V_P as from Sakamaki *et al.* [2016], we match PREM value of V_P for ~ 1
294 wt.% Si at 6300 K and ~ 2 wt.% Si at 7300 K. The last solution is not acceptable as a Fe-Si
295 alloy is not solid at such a high temperatures [Morard *et al.*, 2011; Anzellini *et al.*, 2013].
296 Furthermore, irrespectively whether we assume a temperature effect on V_S of $\sim -0.33 \text{ m/s K}^{-1}$
297 (as from estimates from calculations on pure Fe and a Fe-Si alloy with 3.2 wt.% Si), or $\sim -$
298 0.23 m/s K^{-1} (as from estimates from calculations on Fe-Si alloy with 6,7 wt.% Si), or ~ -0.24
299 m/s K^{-1} for V_S (scaling the estimates from calculations on pure Fe in line with the reduced
300 effect on V_P), there is no obvious solution matching PREM values of V_P and V_S for a fixed Si
301 content. Further, improved constraints on temperature effects on sound velocities remain
302 crucial to reliably estimate the Si content in the inner core.

303

304 **5. Conclusions**

305 We carried out sound velocity and density measurements on solid hcp-Fe and an hcp-
306 Fe-Si alloy with 9 wt.% Si up to ~ 170 and ~ 140 GPa, respectively. The experimentally
307 established $V_{P-\rho}$ and $V_{S-\rho}$ relations for pure Fe are in good agreement with results from ab
308 initio calculations and clearly show that within uncertainties both compressional and shear
309 velocity at 300 K scale linearly with density (Figure 4). At 300 K and at the inner core density
310 of 13000 kg/m^3 reference values for V_P and V_S are respectively $11680 \pm 250 \text{ m/s}$ and
311 $5890 \pm 360 \text{ m/s}$. Measurements on the Fe-Si alloy with 9 wt.% Si allowed us to discriminate
312 between previous inconsistent datasets (Figure 5) and to propose $V_{P-\rho}$ and $V_{S-\rho}$ relations for
313 Fe-Si9. These results are used to address the presence and abundance of Si in the Earth's
314 inner core.

315 From a methodological standpoint, constraints coming only from density [e.g. *Tateno et*
316 *al., 2015*] or even by combined density and compressional sound velocity [e.g. *Badro et al.,*
317 *2007; Mao et al., 2012; Ohtani et al., 2013*] can be used to exclude possibilities, but it is
318 necessary to simultaneously consider V_P , V_S and ρ to propose a consistent composition for the
319 Earth's inner core. Qualitatively, at inner core conditions, high temperature reduces sound
320 velocities, even at constant density, while Si alloying at level of 9 wt.%, besides reducing ρ ,
321 increases V_P and decreases V_S with respect to pure Fe. These same effects have been very
322 recently suggested by calculations on Fe-Si alloys [*Martorell et al., 2016*], as well as for
323 carbon alloying [*Caracas, 2017*]. Assuming an ideal linear mixing model to be valid for low
324 to moderate Si concentration ($< 10 \text{ wt.}\%$), we quantitatively evaluate the effect in $\sim +80 \text{ m/s}$ on
325 V_P and $\sim -80 \text{ m/s}$ on V_S for each wt.% of Si at the inner core density of 13000 kg/m^3 . Studies
326 on samples of intermediate compositions will allow further refinement of this estimation.

327 We explored the possible solutions for an hcp-Fe-Si alloy whose density, compressional
328 and shear sound velocities would match PREM values for pressures in the 330 to 360 GPa

329 range and temperatures in the 4000 to 7500 K range. The existence of a solution and the
330 amount of Si justifying the seismological observations strongly depends on the way we model
331 anharmonic effects on sound velocities at high temperature and on core temperature. In
332 particular we obtain possible solutions only for large temperature corrections, relatively high
333 core temperatures (T between 6200 and 6500 K) and for Si content not exceeding 3 ± 1 wt.%
334 Si. Accordingly, the current results do not support presence of Si in the inner core at level of 6
335 to 8 wt.% [*Mao et al., 2012; Fischer et al., 2015; Tateno et al., 2015*], while on the solely
336 basis of density and sound velocities, we cannot discriminate between results proposing little
337 (up to 4 wt.%) [e.g. *Badro et al., 2007; Antonangeli et al., 2010*] to no presence [*Martorell et*
338 *al., 2016*] of Si in the inner core. More experimental and theoretical work on Fe-Si alloys to
339 extend the directly probed pressure and temperature range and to check the limit of the ideal
340 mixing approximation remains to be performed. We also encourage performing calculations
341 not only at actual core conditions, but as well at conditions where experimental data exist, so
342 as to validate theoretical treatments of alloys.

343

344 **Acknowledgments**

345 This work was supported by the Investissements d'Avenir programme (reference ANR-
346 11-IDEX-0004-02) and more specifically within the framework of the Cluster of Excellence
347 MATériaux Interfaces Surfaces Environnement (MATISSE) led by Sorbonne Universités
348 (grant to DA). The research was also supported by the Carnegie Institution for Science and
349 NASA (grant to YF). Authors wish to thank Sébastien Merkel for discussion about texture
350 and preferential orientations.

351

352 **References**

353 Antonangeli, D., F. Occelli, H. Requardt, J. Badro, G. Fiquet, M. Krisch (2004), Elastic
354 anisotropy in textured hcp-iron to 112 GPa from sound wave propagation measurements,
355 *Earth Planet. Sci. Lett.* 225, 243–251.

356 Antonangeli, D., J. Siebert, J. Badro, D.L. Farber, G. Fiquet, G. Morard, F.J. Ryerson (2010),
357 Composition of the Earth’s inner core from high-pressure sound velocity measurements
358 in Fe–Ni–Si alloys, *Earth Planet. Sci. Lett.* 295, 292–296.

359 Antonangeli, D., T. Komabayashi, F. Occelli, E. Borissenko, A.C. Walters, G. Fiquet, Y. Fei,
360 (2012), Simultaneous sound velocity and density measurements of hcp iron up to 93
361 GPa and 1100 K: An experimental test of the Birch’s law at high temperature, *Earth*
362 *Planet. Sci. Lett.* 331-332, 210–214.

363 Antonangeli, D., and E. Ohtani (2015), Sound velocity of hcp-Fe at high pressure: exper-
364 imental constraints, extrapolations and comparison with seismic models, *Prog. Earth*
365 *Planet. Sci.* 2, 3.

366 Antonangeli, D., G. Morard, N.C. Schmerr, T. Komabayashi, M. Krisch, G. Fiquet, Y. Fei
367 (2015), Toward a mineral physics reference model for the Moon’s core, *Proc. Natl.*
368 *Acad. Sci. USA* 112, 3916–3919.

369 Anzellini, S., A. Dewaele, M. Mezouar, P. Loubeyre, G. Morard (2013), Melting of iron at
370 Earth’s inner core boundary based on fast x-ray diffraction, *Science* 340, 464–466.

371 Badro, J., G. Fiquet, F. Guyot, E. Gregoryanz, F. Occelli, D. Antonangeli, M. d’Astuto (2007),
372 Effect of light elements on the sound velocities in solid iron: implications for the
373 composition of Earth’s core, *Earth Planet. Sci. Lett.* 254, 233–238.

374 Birch, F. (1952). Elasticity and constitution of the Earth’s interior, *J. Geophys. Res.* 57, 227–
375 286.

376 Bosak, A., M. Krisch, I. Fischer, S. Huotari, G. Monaco (2007), Inelastic x-ray scattering
377 from polycrystalline materials at low momentum transfer, *Phys. Rev. B* 75, 064106.

378 Bosak, A., M. Krisch, A. Chumakov, I.A. Abrisokov, L. Dubrovinsky (2016), Possible
379 artifacts in inferring seismic properties from X-ray data, *Phys. Earth Planet. Inter.* 260,
380 14–19.

381 Caracas, R. (2017). The influence of carbon on the seismic properties of solid iron, *Geophys.*
382 *Res. Lett.* 44, 128–134.

383 Crowhurst, J.C., A.F. Goncharov, J.M. Zaug (2004), Impulsive stimulated light scattering
384 from opaque materials at high pressure, *J. Phys. Condens. Matter.* 16, S1137–S1142.

385 Decremps, F., D. Antonangeli, M. Gauthier, S. Ayrinhac, M. Morand, G. Le Marchand, F.
386 Bergame, J. Philippe (2014), Sound velocity measurements of iron up to 152 GPa by
387 picosecond acoustics in diamond anvil cell, *Geophys. Res. Lett.* 41, 1459.

388 Dziewonski, A.M., and D.L. Anderson (1981). Preliminary reference Earth model, *Phys.*
389 *Earth Planet. Inter.* 25, 297–356.

390 Fiquet, G., J. Badro, F. Guyot, H. Requardt, M. Krisch (2001). Sound velocities in iron to 110
391 gigapascals, *Science* 291, 468–471.

392 Fiquet, G., J. Badro, E. Gregoryanz, Y. Fei, F. Occelli (2009). Sound velocity in iron carbide
393 (Fe_3C) at high pressure: Implications for the carbon content of the Earth's inner core,
394 *Phys. Earth Planet. Inter.* 172, 125–129.

395 Fischer, R.A., Y. Nakajima, A.J. Campbell, D.J. Frost, D. Harries, F. Langenhorst, N.
396 Miyajima, K. Pollok, D.C. Rubie (2015), High pressure metal–silicate partitioning of Ni,
397 Co, V, Cr, Si, and O, *Geochim. Cosmochim. Acta* 167, 177–194.

398 Fei, Y. (2017). Unpublished data.

399 Fei, Y., C. Murphy, Y. Shibasaki, A. Shahar, and H. Huang (2016), Thermal equation of state
400 of hcp-iron: Constraint on the density deficit of Earth's solid inner core, *Geophys. Res.*
401 *Lett.* *43*, 6837–6843.

402 Gleason, A.E., W.L. Mao, J.Y. Zhao (2013), Sound velocities for hexagonally closepacked
403 iron compressed hydrostatically to 136 GPa from phonon density of states, *Geophys.*
404 *Res. Lett.* *40*, 2983–2987.

405 Guinan, M.W., and D.N. Beshers (1968), Pressure derivatives of the elastic constants of α -
406 iron to 110 kbs, *J. Phys. Chem. Solids* *29*, 541–549.

407 Lin, J.-F., V.V. Struzhkin, W. Sturhahn, E. Huang, J. Zhao, Y.H. Hu, E.E. Alp, H.-K. Mao, N.
408 Boctor, J. Hemley (2003), Sound velocities of iron–nickel and iron–silicon alloys at
409 high pressures. *Geophys. Res. Lett.* *30*, 2112.

410 Liu, J., J.-F. Lin, A. Alatas, A., M.Y. Hu, J. Zhao, L. Dubrovinsky (2016), Seismic parameters
411 of hcp-Fe alloyed with Ni and Si in the Earth's inner core, *J. Geophys. Res. Solid Earth*
412 *121*, 610–623.

413 Mao, H.K., Y. Wu, L.C. Chen, J.F. Shu, A.P. Jephcoat (1990), Static compression of iron to
414 300 GPa and Fe_{0.8}Ni_{0.2} alloy to 260 GPa: Implications for composition of the core, *J.*
415 *Geophys. Res.* *95*, 21737-21742.

416 Mao, H.K., J. Shu, G. Shen, R.J. Hemley, B. Li, A.K. Singh (1998), Elasticity and rheology of
417 iron above 220 GPa and the nature of the Earth's inner core. *Nature* *396*, 741–743;
418 correction (1999) *Nature* *399*, 80.

419 Mao, Z., J.-F. Lin, J. Liu, A. Alatas, L. Gao, J. Zhao, H.-K. Mao (2012), Sound velocities of
420 Fe and Fe–Si alloy in the Earth's core, *Proc. Natl. Acad. Sci. USA* *109*, 10239–10244.

421 Martorell, B., L. Vočadlo, J. Brodholt, I.G. Wood (2013), Strong pre-melting effect in the
422 elastic properties of hcp-Fe under inner-core conditions, *Science* *342*, 466–468.

423 Martorell, B., I.G. Wood, J., Brodholt, L. Vočadlo (2016), The elastic properties of hcp-
424 $\text{Fe}_{1-x}\text{Si}_x$ at Earth's inner-core conditions, *Earth Planet. Sci. Lett.* 451, 89–96.

425 Merkel, S., N. Miyajima, D. Antonangeli, G. Fiquet, T. Yagi (2006). Lattice preferred
426 orientation and stress in polycrystalline hcp-Co plastically deformed under high
427 pressure, *J. Appl. Phys.* 100, 023510.

428 Morard, G., D. Andrault, N. Guignot, J. Siebert, G. Garbarino, D. Antonangeli (2011),
429 Melting of Fe-Ni-Si and Fe-Ni-S alloys at megabar pressures: implications for the core-
430 mantle boundary temperature, *Phys. Chem. Minerals* 38, 767–776.

431 Murphy, C.A., J.M. Jackson, W. Sturhahn (2013), Experimental constraints on the
432 thermodynamics and sound velocities of hcp-Fe to core pressures, *J. Geophys. Res.*
433 *Solid Earth* 118, 1–18.

434 Ohtani, E., Y. Shibazaki, T. Sakai, K. Mibe, H. Fukui, S. Kamada, T. Sakamaki, Y. Seto, S.
435 Tsutsui, A.Q.R. Baron (2013), Sound velocity of hexagonal close-packed iron up to
436 core pressures, *Geophys. Res. Lett.* 40, 5089–5094.

437 Prescher, C., and V.B. Prakapenka (2015), DIOPTAS: a program for reduction of two-
438 dimensional X-ray diffraction data and data exploration, *High Pressure Research* 35,
439 223–230.

440 Sakai, T., S. Takahashi, N. Nishitani, I. Mashini, E. Ohtani, N. Hirao (2014), Equation of state
441 of pure iron and Fe_{0.9}Ni_{0.1} alloy up to 3 Mbar, *Phys. Earth Planet. Inter.* 228, 114–126.

442 Sakairi, T., T. Sakamaki, E. Ohtani, H. Fukui, S. Kamada, S. Tsutsui, H. Uchiyama, A.Q.R.
443 Baron (2017), *American Mineralogist*, in press. DOI: [http://dx.doi.org/10.2138/am-](http://dx.doi.org/10.2138/am-2018-6072)
444 [2018-6072](http://dx.doi.org/10.2138/am-2018-6072).

445 Sakamaki, T., E. Ohtani, H. Fukui, S. Kamada, S. Takahashi, T. Sakairi, A. Takahata, T.
446 Sakai, S. Tsutsui, D. Ishikawa, R. Shiraishi, Y. Seto, T. Tsuchiya, A.Q.R. Baron (2016),

447 Constraints on Earth's inner core composition inferred from measurements of the sound
448 velocity of hcp-iron in extreme conditions, *Sci. Adv.* 2, e1500802.

449 Sha, X., and R.E. Cohen (2010), Elastic isotropy of ϵ -Fe under Earth's core conditions,
450 *Geophys. Res. Lett.* 37, L10302.

451 Siebert, J., J. Badro, D. Antonangeli, F.J. Ryerson (2013), Terrestrial accretion under
452 oxidizing conditions, *Science* 339, 1194–1197.

453 Tateno, S., K. Hirose, Y. Ohishi, Y. Tatsumi (2010), The structure of iron in the Earth's core,
454 *Science* 330, 359–361.

455 Tateno, S., Y. Kuwayama, K. Hirose, Y. Ohishi (2015), The structure of Fe-Si alloy in the
456 Earth's inner core, *Earth Planet. Sci. Lett.* 418, 11–19.

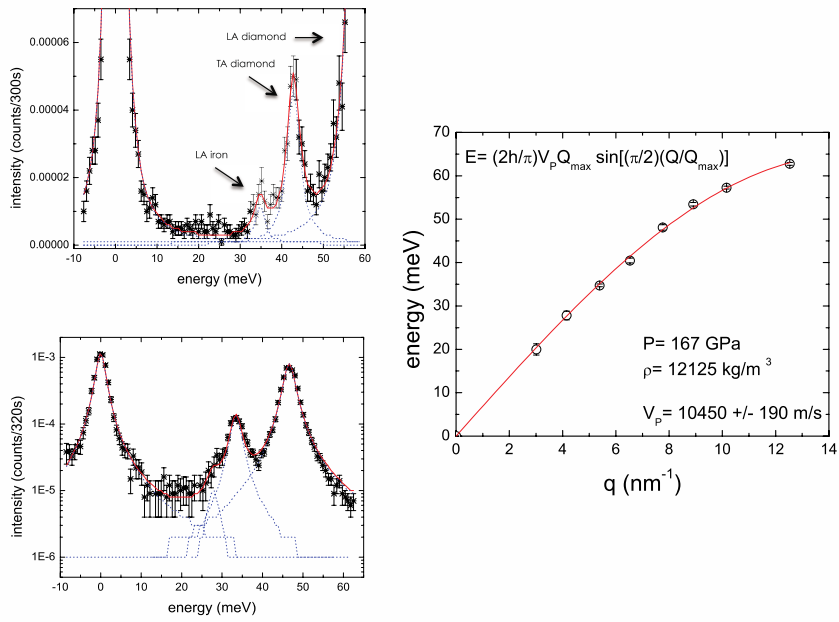
457 Tsuchiya, T., and M. Fujibuki (2009), Effects of Si on the elastic property of Fe at Earth's
458 inner core pressures: First principles study, *Phys. Earth Planet. Inter.* 174, 212–219.

459 Vočadlo, L., D. Dobson, I.G. Wood (2009), Ab initio calculations of the elasticity of hcp-Fe
460 as a function of temperature at inner-core pressure, *Earth Planet. Sci. Lett.* 288, 534–
461 538.

462 Wenk, H.R., S. Matthies, R.J. Hemley, H.-K. Mao, J. Shu (2000), The plastic deformation of
463 iron at pressures of the Earth's inner core, *Nature* 405, 1044–1047.

464 Wenk, H.R., I. Lonardelli, S. Merkel, L. Miyagi, J. Pehl, S. Speziale, C.E. Tommaseo (2006),
465 Deformation textures produced in diamond anvil experiments, analyzed in radial
466 diffraction geometry, *J. Phys.: Cond. Matter* 18, S933–S947.

467



468

469

Figure 1. Examples of IXS spectra (left) and aggregate phonon dispersion (right)

470

obtained for pure-Fe at the highest investigated pressure ($\rho=12125 \text{ kg/m}^3$, corresponding to

471

$\sim 167 \text{ GPa}$). Up left: IXS spectrum for $q=5.39 \text{ nm}^{-1}$; bottom left IXS spectrum for $q=4.15 \text{ nm}^{-1}$.

472

IXS spectra are characterized by an elastic line, centered around zero, and inelastic features,

473

assigned for increasing energy to the longitudinal acoustic (LA) aggregate phonon of iron

474

and the transverse acoustic (TA) and longitudinal acoustic (LA) phonons of diamond. The

475

experimental points and error bars are shown together with the best-fit (red line) and

476

individual excitations (dashed blue lines). Sample phonons for q of 5.39 nm^{-1} and higher are

477

well resolved and visible in linear scale, while for smaller q values, sample phonons and TA

478

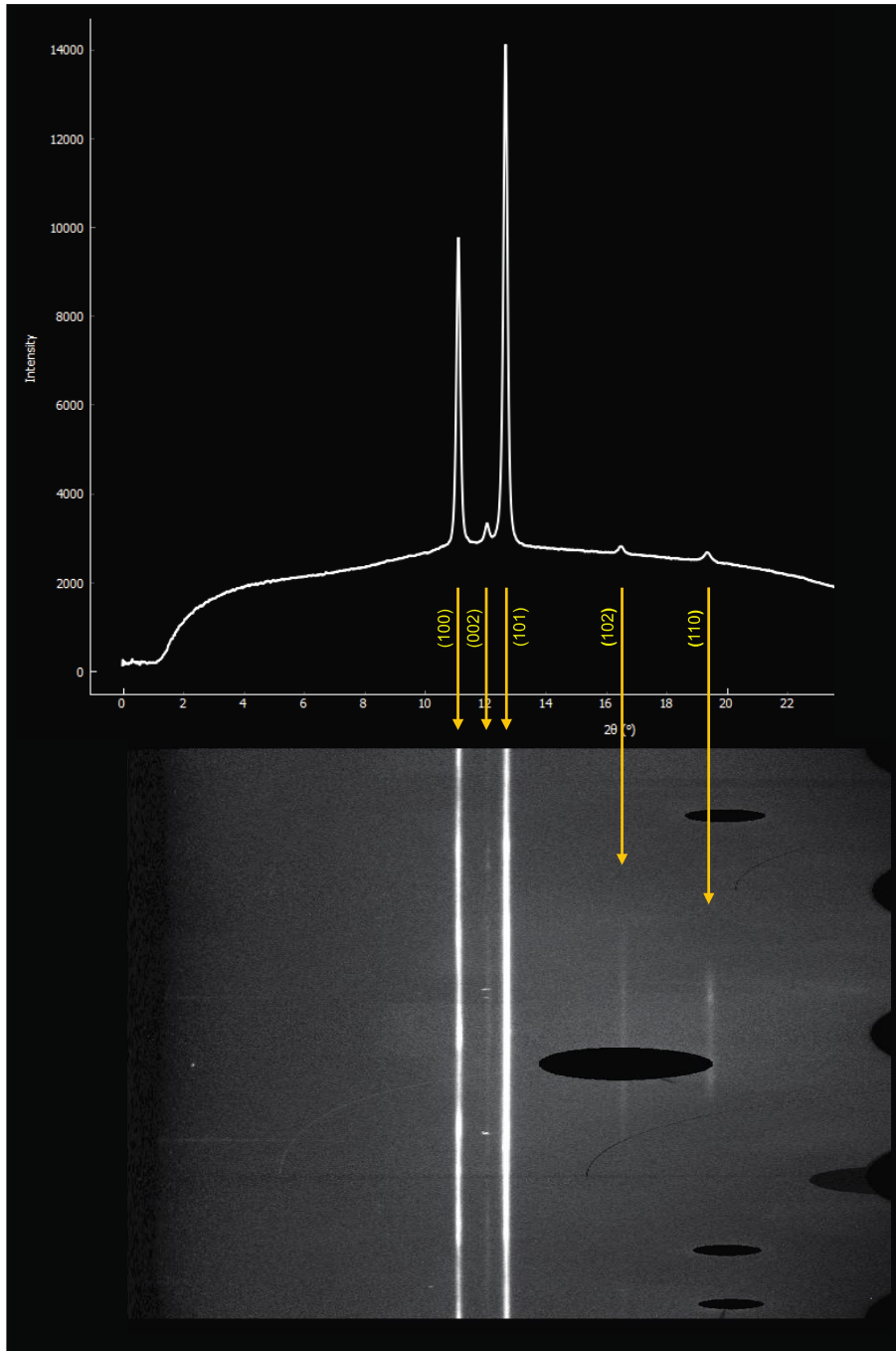
phonon of diamonds get very close, and sample phonons become a shoulder on the low-

479

energy side of the TA phonon of diamond, better visible in logarithmic scale.

480

481

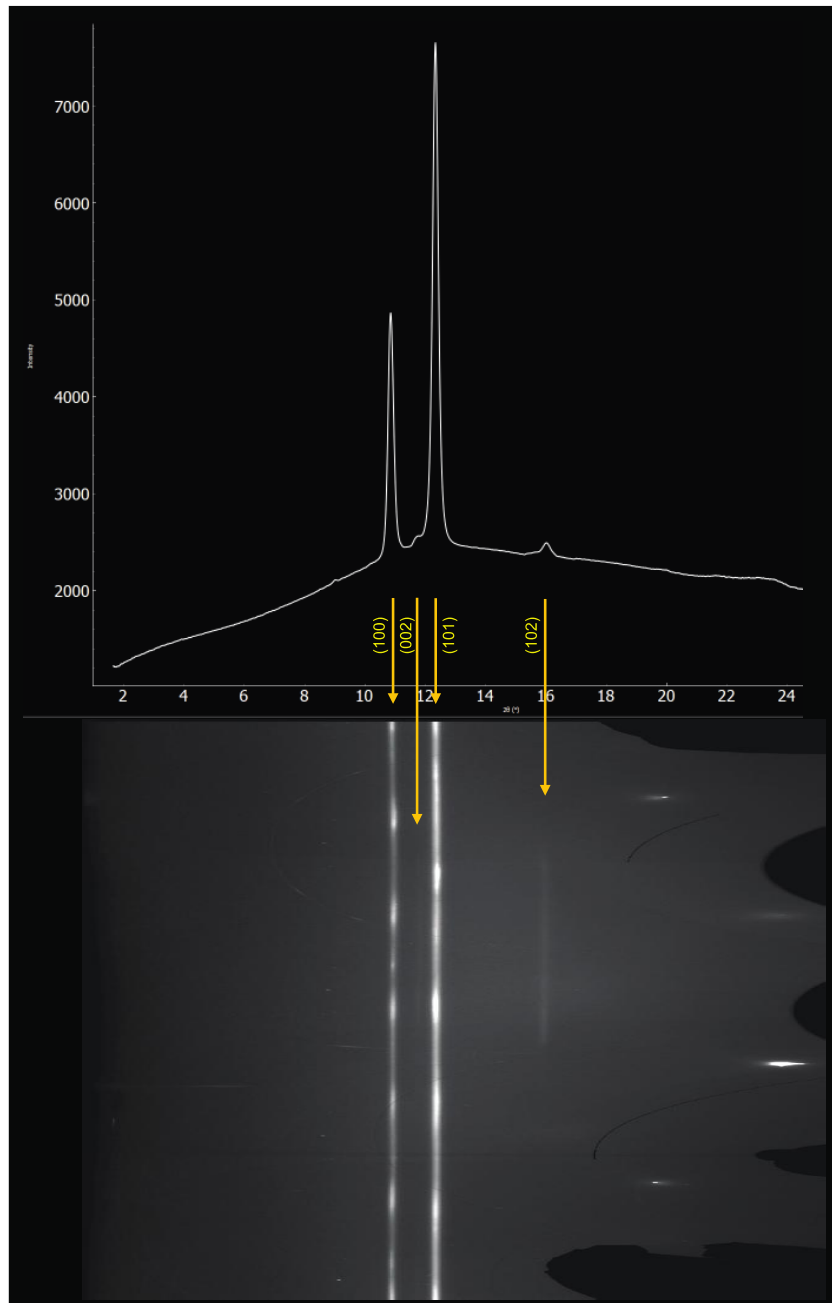


482

483 *Figure 2. Example of integrated diffraction pattern collected on pure hcp-Fe at*
 484 *P~167 GPa (top) and caked into a rectilinear projection (bottom). 2D diffraction images*
 485 *have been integrated using Dioptas [Prescher and Prakapenka, 2015].*

486

487



488

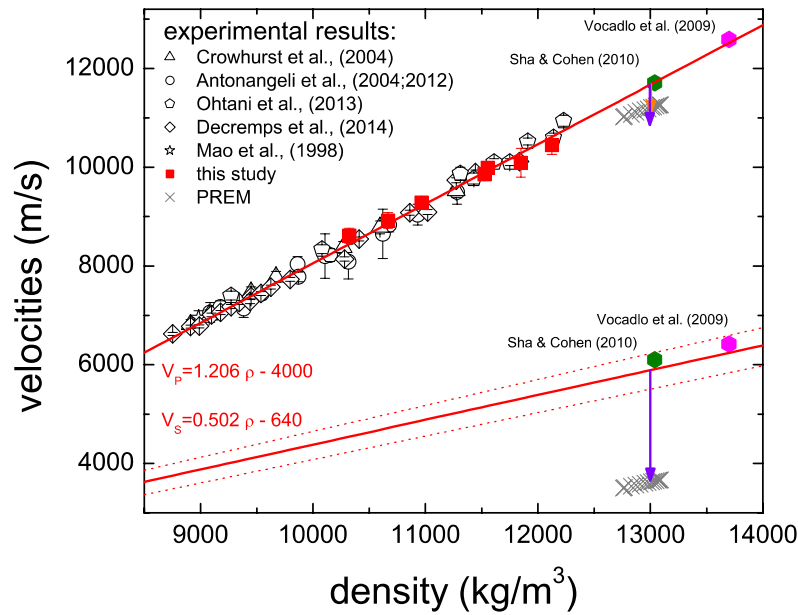
489 *Figure 3. Example of integrated diffraction pattern collected on hcp-FeSi9 at P~117*

490 *GPa (top) and caked into a rectilinear projection (bottom). 2D diffraction images have been*

491 *integrated using Dioptas [Prescher and Prakapenka, 2015].*

492

493

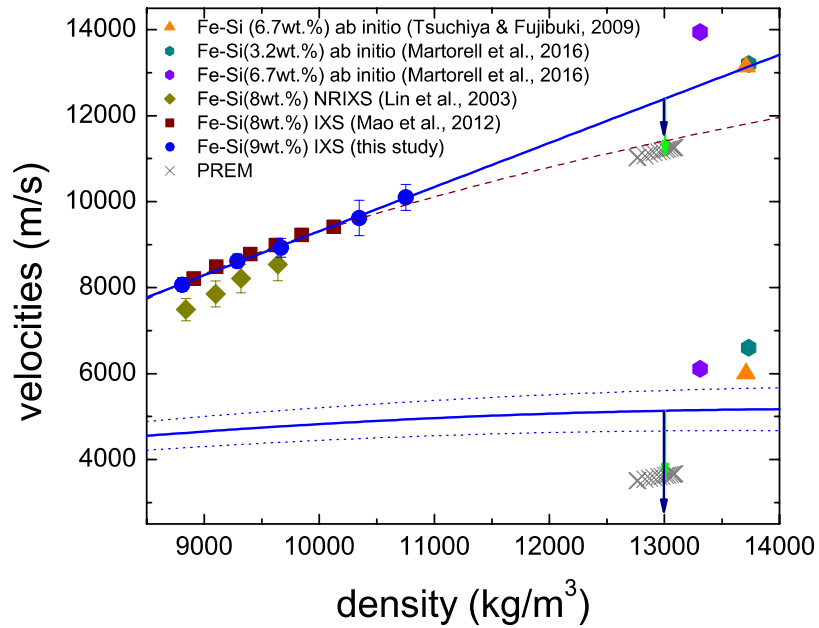


494

495 **Figure 4. Aggregate compressional (V_P) and shear (V_S) sound velocities of hcp-Fe at**
 496 **300 K as a function of density.** Results of this study are compared with a selection of
 497 published measurements at 300 K [Mao et al., 1998; Crowhurst et al., 2004; Antonangeli et
 498 al., 2004, 2012; Ohtani et al., 2013; Decremps et al., 2014] (for further details see
 499 Antonangeli and Ohtani [2015]), ab initio calculations at 0 K and 295 GPa [Vočadlo et al.,
 500 2009] and at 0 K and 13040 kg/m³ [Sha and Cohen, 2010]. PREM [Dziewonski and Anderson,
 501 1981] is reported as crosses. Solid lines show the established linear V_P - ρ and V_S - ρ
 502 relationships. Dotted lines show confidence level on the derived V_S . Arrows indicate possible
 503 magnitude of anharmonic effects up to 7000 K (see text).

504

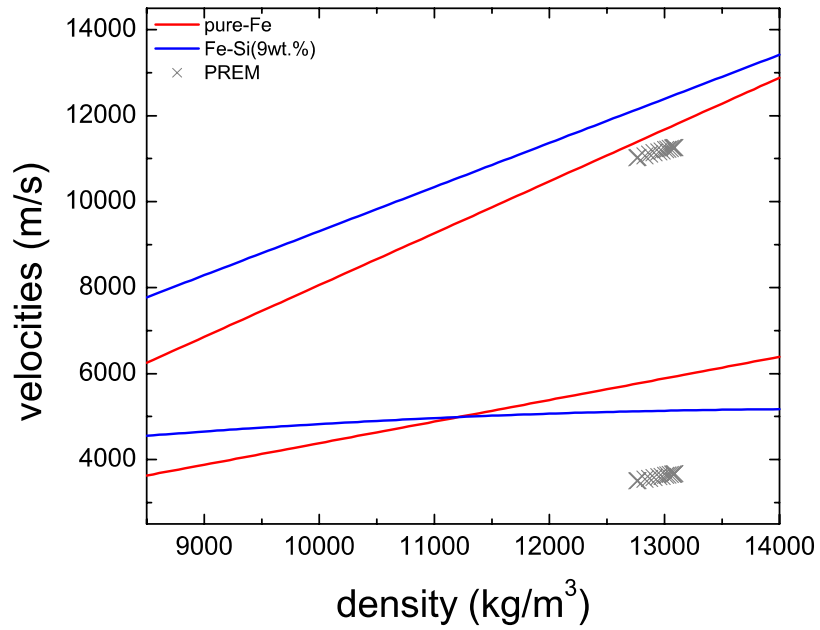
505



506

507 *Figure 5. Aggregate compressional (V_P) and shear (V_S) sound velocities of hcp-Fe-*
508 *Si9 at 300 K as a function of density. Results of this study are compared with measurements*
509 *at 300 K on a hcp-Fe-Si alloy with 8 wt.% Si by NRIXS [Lin et al., 2003] and by IXS [Mao et*
510 *al., 2012] as well as with results of ab initio calculations at 0 K and 360 GPa on an hcp-Fe-Si*
511 *alloy with 6.7 wt.% Si [Tsuchiya and Fujibuki, 2009] and at 0 K and 360 GPa on hcp-Fe-Si*
512 *alloys with 3.2 and 6.7 wt.% Si [Martorell et al., 2016]. PREM [Dziewonski and Anderson,*
513 *1981] is reported as crosses. Solid lines show the proposed $V_{P-\rho}$ ($V_P=1.026\times\rho-946$) and $V_{S-\rho}$*
514 *($V_S=1530+0.503\times\rho-1.736\times 10^{-5}\times\rho^2$) relationships. Dotted lines show confidence level on the*
515 *derived V_S . The dashed line is the empirical power-law function used by Mao et al., [2012] to*
516 *describe their $V_{P-\rho}$ data. Arrows indicate possible magnitude of anharmonic effects up to*
517 *7000 K (see text).*

518



519

520 *Figure 6. Comparison of the here-proposed density dependence of the aggregate*
 521 *compressional (V_p) and shear (V_s) sound velocities of hcp-Fe and hcp-FeSi9 extrapolated*
 522 *to core density. PREM [Dziewonski and Anderson, 1981] is reported as crosses.*

523

524

525

526

527 **Table 1. Measured densities and compressional sound velocities (V_P).** Pressure
528 *estimated from measured diffraction patterns are reported as well. See text for discussion of*
529 *pressure uncertainties and pressure gradients. Assuming different equation of state for hcp-*
530 *Fe leads to a maximum difference in the reported pressure of less than 10 GPa at the highest*
531 *density when using equation of state from Mao et al., [1990].*

Sample	Density (kg/m³)	Pressure (GPa)	V_P (m/s)
hcp-Fe	10325	63	8610±150
hcp-Fe	10665	79	8920±160
hcp-Fe	10965	96	9280±90
hcp-Fe	11525	124	9860±110
hcp-Fe	11555	126	9990±120
hcp-Fe	11850	146	10090±290
hcp-Fe	12125	167	10450±190
hcp-Fe-Si9 ^a	8805	42	8070±170
hcp-Fe-Si9	9285	59	8620±160
hcp-Fe-Si9	9665	79	8930±220
hcp-Fe-Si9	10350	117	9620±410
hcp-Fe-Si9	10755	144	10100±300

532 ^a This point have been collected on decompression.

533